

PAPER

Electrochemical and mechanical performance of reduced graphene oxide, conductive hydrogel, and electrodeposited Pt–Ir coated electrodes: an active *in vitro* study

To cite this article: Ashley N Dalrymple *et al* 2020 *J. Neural Eng.* **17** 016015

View the [article online](#) for updates and enhancements.

You may also like

- [The role of lubricants, scanning velocity and operating environment in adhesion, friction and wear of Pt–Ir coated probes for atomic force microscope probe-based ferroelectric recording technology](#)
Bharat Bhushan and Kwang Joo Kwak
- [High-reliability graphene-wrapped nanoprobes for scanning probe microscopy](#)
Liang Cao, Ri Liu, Wenxiao Zhang *et al.*
- [In-Situ Analysis of Voltage Losses at the Porous Transport Layer in a PEM Water Electrolyzer Cell](#)
Zhenye Kang, Shaun M Alia and Guido Bender

Recent citations

- [The Influence of Physicochemical Properties on the Processibility of Conducting Polymers: A Bioelectronics Perspective](#)
Julian Heck *et al*
- [Tao Sun *et al*](#)
- [Platinum dissolution and tissue response following long-term electrical stimulation at high charge densities](#)
Robert K Shepherd *et al*



PAPER

Electrochemical and mechanical performance of reduced graphene oxide, conductive hydrogel, and electrodeposited Pt–Ir coated electrodes: an active *in vitro* study

RECEIVED
19 July 2019REVISED
24 October 2019ACCEPTED FOR PUBLICATION
25 October 2019PUBLISHED
23 December 2019

Ashley N Dalrymple¹ , Mario Huynh¹, Ulises Aregueta Robles³ , Jason B Marroquin⁴, Curtis D Lee⁵, Artin Petrossians³, John J Whalen III⁵, Dan Li⁶, Helena C Parkington⁷, John S Forsythe⁴ , Rylie A Green⁸, Laura A Poole-Warren³, Robert K Shepherd^{1,2}  and James B Fallon^{1,2,9,10} 

¹ Bionics Institute, St. Vincent's Hospital, Melbourne, VIC, Australia

² Medical Bionics Department, University of Melbourne, Melbourne, VIC, Australia

³ Graduate School of Biomedical Engineering, University of New South Wales, Sydney, NSW, Australia

⁴ Department of Materials Science and Engineering, Monash Institute of Medical Engineering, Monash University, Melbourne, VIC, Australia

⁵ Platinum Group Coatings, LLC., Pasadena, CA, United States of America

⁶ Department of Chemical Engineering, University of Melbourne, Melbourne, VIC, Australia

⁷ Department of Physiology, Biomedicine Discovery Institute, Monash University, Melbourne, VIC, Australia

⁸ Department of Bioengineering, Imperial College London, London, England

⁹ Author to whom any correspondence should be addressed.

¹⁰ Bionics Institute, 384-388 Albert Street, East Melbourne, VIC, Australia

E-mail: jfallon@bionicsinstitute.org

Keywords: electrical stimulation, neural prosthesis, electrode, *in vitro*, accelerated aging

Abstract

Objective. To systematically compare the *in vitro* electrochemical and mechanical properties of several electrode coatings that have been reported to increase the efficacy of medical bionics devices by increasing the amount of charge that can be delivered safely to the target neural tissue. **Approach.** Smooth platinum (Pt) ring and disc electrodes were coated with reduced graphene oxide, conductive hydrogel, or electrodeposited Pt–Ir. Electrodes with coatings were compared with uncoated smooth Pt electrodes before and after an *in vitro* accelerated aging protocol. The various coatings were compared mechanically using the adhesion-by-tape test. Electrodes were stimulated in saline for 24 hours/day 7 days/week for 21 d at 85 °C (1.6-year equivalence) at a constant charge density of 200 $\mu\text{C}/\text{cm}^2/\text{phase}$. Electrodes were graded on surface corrosion and trace analysis of Pt in the electrolyte after aging. Electrochemical measurements performed before, during, and after aging included electrochemical impedance spectroscopy, cyclic voltammetry, and charge injection limit and impedance from voltage transient recordings. **Main results.** All three coatings adhered well to smooth Pt and exhibited electrochemical advantage over smooth Pt electrodes prior to aging. After aging, graphene coated electrodes displayed a stimulation-induced increase in impedance and reduction in the charge injection limit ($p < 0.001$), alongside extensive corrosion and release of Pt into the electrolyte. In contrast, both conductive hydrogel and Pt–Ir coated electrodes had smaller impedances and larger charge injection limits than smooth Pt electrodes ($p < 0.001$) following aging regardless of the stimulus level and with little evidence of corrosion or Pt dissolution. **Significance.** This study rigorously tested the mechanical and electrochemical performance of electrode coatings *in vitro* and provided suitable candidates for future *in vivo* testing.

Introduction

Medical bionics devices can be used to interact with the nervous system through electrical stimulation and/or recording to restore lost function and improve quality of life. For example, cochlear implants have been widely used to restore hearing to profoundly deaf children and adults who have been deaf for decades (Clark 2003, Zeng *et al* 2008). Ring electrodes, such as those used in cochlear implants, are similar to electrodes used for deep brain stimulation (Amon and Alesch 2017) and spinal cord stimulation (Verrills *et al* 2016). Paddle arrays, containing disc electrodes, can also be used for a variety of applications including cortical recordings (Woo-Ram *et al* 2017), spinal cord stimulation (Barolat *et al* 2001, Chang *et al* 2014), as well as restoring vision as a retinal prosthesis (Bin *et al* 2017, Abbott *et al* 2018). The electrodes on these arrays are typically made of platinum (Pt) or iridium (Ir), which are effective for chronic implants because they are generally stable and biocompatible (Burgio 1986, Stover and Lenarz 2009). The spatial specificity of stimulation achieved with implanted devices can be improved by increasing the number of electrodes and/or by making them smaller in size. However, to continue to produce the desired functions using smaller electrodes, the charge density increases closer to, or beyond, the safe water window limit, which is defined as the potential that results in the electrolysis of water (Cogan 2008). To remain within the safe water window and to continue to target the desired neural cells, coatings can be used to reduce the impedance and increase the charge injection capacity of the electrodes.

Many potential electrode materials are being developed with properties that include increased mechanical compliance with neural tissue and a significant increase in charge injection capacity over conventional electrode materials such as Pt (Richardson *et al* 2009, Ludwig *et al* 2011, Venkatraman *et al* 2011, Hassarati *et al* 2014, Green and Abidian 2015, Zeng *et al* 2015, Bennett *et al* 2016, Ouyang *et al* 2017, Nimbalkar *et al* 2018). These materials can be directly coated onto the metal substrate. While promising, many of these coatings delaminate from the metal substrate during long-term electrical stimulation (Green *et al* 2012a, Boehler *et al* 2017, Ouyang *et al* 2017) resulting in a loss of their electrochemical advantage.

In addition to standard electrochemical evaluation, it is important to assess the adhesive properties of coatings using well controlled mechanical tests before committing resources to extensive *in vivo* testing (Shepherd *et al* 2018). Moreover, it is imperative that the coatings remain intact and effective over a long period of time, as the intention of medical bionics devices is to remain implanted for the user's lifetime.

To understand the relative performance of a range of potential electrode materials including reduced graphene oxide, conductive hydrogel, and electrodeposited Pt–Ir, in a side-by-side comparison, an

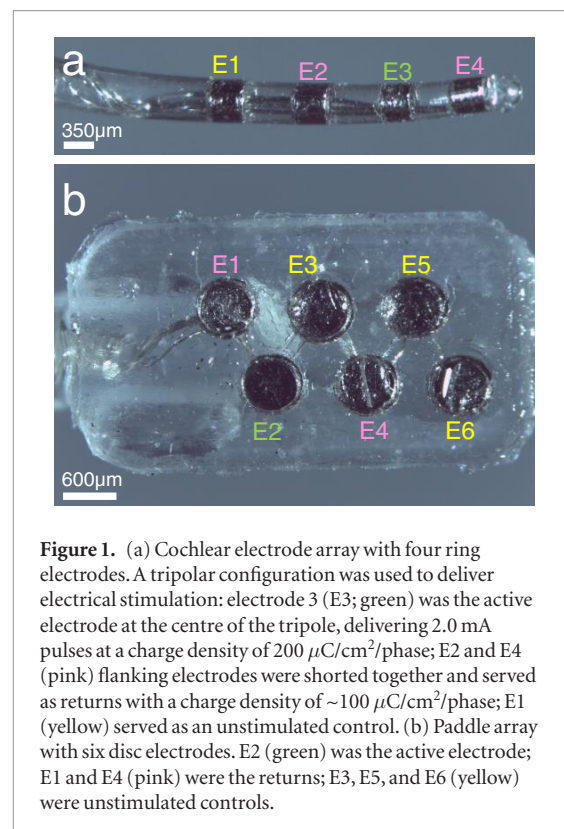


Figure 1. (a) Cochlear electrode array with four ring electrodes. A tripolar configuration was used to deliver electrical stimulation: electrode 3 (E3; green) was the active electrode at the centre of the tripole, delivering 2.0 mA pulses at a charge density of $200 \mu\text{C}/\text{cm}^2/\text{phase}$; E2 and E4 (pink) flanking electrodes were shorted together and served as returns with a charge density of $\sim 100 \mu\text{C}/\text{cm}^2/\text{phase}$; E1 (yellow) served as an unstimulated control. (b) Paddle array with six disc electrodes. E2 (green) was the active electrode; E1 and E4 (pink) were the returns; E3, E5, and E6 (yellow) were unstimulated controls.

in vitro study was undertaken. Each of these materials has previously shown promising results by lowering the impedance of the electrodes (Bennett *et al* 2016, Goding *et al* 2017a, Lee *et al* 2018). This accelerated aging study was designed to evaluate the mechanical and electrochemical performance of materials coated onto Pt ring and disc electrodes and compared them to conventional smooth Pt electrodes.

Methods

Fabrication of electrode arrays

Two types of electrode arrays were used in the present study (i) a cochlear implant design that incorporated 4 to 22 Pt ring electrodes along a tapered longitudinal array; and (ii) a flat paddle design incorporating 6 Pt disc electrodes (figure 1). One Pt cochlear implant electrode array was supplied by a commercial cochlear implant manufacturer (Cochlear Ltd., Australia). All other ring electrode arrays were custom made (Bionics Institute, Australia). Pt disc electrodes were manufactured from 99.95% pure $50 \mu\text{m}$ Pt sheet (Goodfellow Cambridge Ltd., U.K.) and laser cut into discs. All electrodes were fabricated on a polydimethylsiloxane (PDMS) insulative carrier and connected to a custom connector via an insulated Pt–Ir leadwire assembly. The geometric surface area for these Pt electrodes from both arrays varied from $0.14\text{--}0.45 \text{ mm}^2$. Two paddle and three cochlear arrays were not coated and served as smooth Pt control arrays for comparisons. In total, 24 electrodes remained uncoated. Three different coatings were applied to disc and ring Pt electrodes (table 1).

Table 1. Number of disc electrodes (on paddle arrays) or ring electrodes (on cochlear arrays) that were coated or uncoated for use in accelerated aging.

Material	Disc electrodes	Ring electrodes	Total
Uncoated smooth Pt	12	12	24
Graphene	12	0	12
Conductive Hydrogel	10	13	33
Pt–Ir	0	10	10

Electrode coatings

Reduced graphene oxide

Electrodeposition of graphene oxide on the Pt surface was performed on two paddle arrays each consisting of six disc electrodes ($N = 12$ electrodes; table 1). The electrodeposition process utilized a saline (0.5 M) electrolyte with suspended graphene oxide (GO_x) (1.5 mg ml^{-1}). A three-electrode configuration was used and a -1.0 V reduction voltage with a scan rate of 10 mV s^{-1} was held for 1 h, driving the GO_x towards the electrodes (Hilder *et al* 2011). This was followed by the direct electrochemical reduction of GO_x to reduced graphene oxide (herein referred to simply as graphene) in a 1.0 M lithium perchlorate (LiClO_4) electrolyte by applying a cyclic voltage reduction ranging from 0 V to -0.8 V at a scan rate of 50 mV s^{-1} (Bennett *et al* 2016).

Conductive hydrogel

Two paddle and two cochlear electrode arrays were coated with conductive hydrogel. Each paddle array had five disc electrodes coated, one cochlear array had four ring electrodes coated, while the other cochlear array had 19 ring electrodes coated ($N = 33$ electrodes; table 1).

Synthesis and fabrication of conductive hydrogel was performed as previously described (Goding *et al* 2017b). Briefly, a pre-layer coat of poly(3,4 ethylenedioxythiophene, PEDOT) doped with para-toluene sulfonate (PEDOT/pTS) was galvanostatically deposited on the electrodes using a two-electrode cell (eDAQ Pty Ltd, NSW, Australia). The PEDOT/pTS monomer solution consisted of 0.1 M EDOT and 0.05 M pTS in a 1:1 ratio of de-ionised (DI) water to acetonitrile. The PEDOT/pTS pre-layer was deposited at 1 mA cm^{-2} for 1 min. The electrode arrays were washed with DI water to remove excess monomer solution and allowed to dry in a laminar flow cabinet overnight.

Poly(vinyl alcohol) (PVA) was chemically modified for incorporation of 5 methacrylate groups and 20 taurine residues per PVA chain (PVA-*taurine*) using previously described methods (Goding *et al* 2017a). A 20 wt% macromer solution of PVA-*taurine* was dissolved in DI water at $80 \text{ }^\circ\text{C}$. Photo-initiator (Irgacure 2959) was added to the macromer solution to achieve a final concentration of 0.1 wt%. The macromer solution was allowed to reach room temperature and then electrode arrays were dip coated with PVA-*taurine*

and immediately crosslinked under ultra-violet light (70 mW cm^{-2} , 336 nm) for 3 min. Following photopolymerisation, PEDOT was galvanostatically deposited through the gel at 0.5 mA cm^{-2} for 20 min. The PEDOT monomer solution consisted of 0.1 M of EDOT in DI water. Samples were washed twice with DI water and placed in a sink of MilliQ water for 24 h to remove unreacted products. Conductive hydrogel coated electrode arrays were then allowed to dry in a laminar flow cabinet for 24 h.

Electrodeposited Pt–Ir

Three cochlear electrode arrays consisting of a total of ten ring electrodes were coated with high surface area Pt–Ir (herein referred to simply as Pt–Ir) using a three-cell potential sweeping electrodeposition technique described previously (Petrossians *et al* 2011a, 2011b) ($N = 10$ electrodes; table 1).

Adhesion testing

The adhesion-by-tape test was used to evaluate the adhesion of each conductive coating prior to undertaking the active *in vitro* study (ASTM 1997, Green *et al* 2012b). Large scale coatings of each material were applied to smooth Pt tiles of $4 \times 4 \text{ mm}$ or larger (being separate samples to the arrays). Using the American Society for Testing and Materials standard as a guideline, the adhesion test was performed by first cutting an 'X' into the coating to expose the underlying metal using a new No. 11 surgical blade. Adhesive tape (ScotchBlue 2080EL, 3M, USA) was placed over the incision for 5 min at room temperature ($\sim 22 \text{ }^\circ\text{C}$) and then carefully removed. The site was examined using a FEI QUANTA 200 scanning electron microscope (SEM) at magnifications of $\times 50$; $\times 200$; $\times 500$ and $\times 1000$ to determine whether there was any delamination of the coating adjacent to the incision line. Test materials were compared with an iridium oxide (IrO_2) coated control manufactured by EIC Laboratories (SIROF electrodes, Boston, MA), as this coating material has been previously shown to withstand the adhesion-by-tape test (Cogan *et al* 2004). Between three and four trials on different tiles were used to evaluate each material.

Accelerated aging

Each electrode array was sealed in a 6 ml glass vial containing 0.9% saline. Accelerated aging was carried out by stimulating 24 hours/day, 7 days/week, except during electrochemical testing, in a MicroClimate chamber (MCB-1.2, Cincinnati Sub-Zero Products, USA) at $85 \text{ }^\circ\text{C}$ and 0% humidity for 21 d (1.6-year equivalence) (Hukins *et al* 2008, ASTM 2011). Throughout the three-week aging protocol, more than 544 million charge balanced biphasic current pulses were delivered through the electrodes over a period of about 500 h. To prevent evaporation of the electrolyte during aging, Teflon tape was wrapped around the threads of the glass containers to externally seal the lid.

The electrodes were connected via cables to custom-built current-controlled stimulators (Senn 2015) that were kept outside of the chamber. Stimuli delivered were charge-balanced biphasic current pulses at a stimulus rate of 300 pulses per second (pps). Current amplitude was fixed for all electrodes at 2.0 mA while the pulse width was adjusted according to the surface area of the electrode to ensure a fixed charge density of $200 \mu\text{C}/\text{cm}^2/\text{phase}$ for all electrodes in the study. This charge density is relatively high and is just below the safe limit of $216 \mu\text{C}/\text{cm}^2/\text{phase}$ for unroughened Pt electrodes (ANSI, 2017). Electrodes were stimulated in a tripolar configuration where a cathodic-first current pulse was delivered to an electrode, referred to as the electrode at the centre of the tripole, while the two flanking electrodes were connected together to provide the return path (figure 1). All current pulses were then reversed in phase two of the pulse (Shepherd *et al* 2019). While the centre electrodes for each tripole developed charge densities of $200 \mu\text{C}/\text{cm}^2/\text{phase}$, the return electrodes developed $\sim 100 \mu\text{C}/\text{cm}^2/\text{phase}$. Charge recovery was achieved using capacitive coupling ($10 \mu\text{F}$) and electrode shorting between current pulses (Patrick *et al* 1990). Additional electrodes on each electrode array served as unstimulated controls.

Electrochemical characterization of electrodes

Electrochemical measurements were made prior to, during, and after the accelerated aging process using the same recording devices throughout. All electrochemical measurements that were collected before and after aging were in Dulbecco's phosphate-buffered saline (DPBS; ThermoFisher Scientific; Massachusetts, USA) at room temperature ($\sim 22^\circ\text{C}$). During aging, the arrays remained in the vials containing saline and were left at room temperature for 2 h prior to completing the electrochemical measurements.

Electrochemical impedance spectroscopy (EIS) measurements were performed using a potentiostat (Interface 1000E, Gamry Instruments, USA). Measurements were made before and after the 21 d aging protocol using a conventional three-electrode setup consisting of a large Pt foil counter electrode (Ionode, AUS), a Ag|AgCl reference electrode (Ionode, AUS), and a working electrode from the arrays in DPBS. Since the electrodes were sealed in saline-filled containers during aging, three-cell measurements were not made during the accelerated aging protocol. Instead, tripolar measurements using the same configuration as for stimulation were made at days 7 and 14, in addition to day 21, of the aging protocol. Frequency spectra ranged from 1 to 100 000 Hz at 10 points/decade with an AC voltage of 50 mV rms. Bode plots (containing the impedance magnitude and phase) and Nyquist plots (containing the real and imaginary components

of the impedance) were generated for each measurement.

Cyclic voltammograms (CVs) were recorded using the same potentiostat used to record EIS by cycling the electrode potential between -0.6 and 0.8 V at a sweep rate of 150 mV s^{-1} . As with the EIS recordings, a three-electrode setup using a Ag|AgCl reference electrode and Pt foil counter electrode was used to collect CVs before and after the 21 d aging protocol, while a tripolar configuration was used to collect CVs during aging. Ten cycles were recorded; the last nine were used for data analysis. CV was performed immediately following the EIS measurement for each electrode. The total charge storage capacity (CSC) was calculated by integrating the area of the average CV curve for each electrode (Cogan 2008). Where voltages are reported, they are with respect to the Ag|AgCl reference electrode potential.

Voltage transient (VT) waveforms were measured (USB-6353, National Instruments, USA) and used to calculate the impedance and charge injection limit (CIL) for each electrode. The VT impedance was determined by applying a single biphasic pulse at $100 \mu\text{A}$ with a pulse width of $100 \mu\text{s}$ and measuring the peak VT at the end of the first phase. Since the pulse delivered to measure the VT impedance was $100 \mu\text{s}$ long, this corresponds to a frequency of 10 kHz. The CIL is defined as the charge that produces a maximum cathodal voltage (E_{mc}) equal to -0.6 V (cathodal limit of the water window for electrolysis of water) (Cogan 2008, Leung *et al* 2015). Electrodes were stimulated with a biphasic charge-balanced cathodic-first current pulse at $100 \mu\text{s}/\text{phase}$ with current amplitudes ranging from $50 \mu\text{A}$ to 2 mA in steps of $50 \mu\text{A}$. E_{mc} was measured by subtracting the access voltage (V_a) from the maximum negative potential. The CIL was calculated using the current immediately below the level that went over the polarization limit of -0.6 V up to a maximum of 2 mA.

The effect of charge density on changes in the CSC, VT impedance, and CIL were compared for each material. If there was more than a 15% change post-aging compared with the pre-aging measurement, then the magnitude of that change outside of the 30% window was computed. This window range was chosen to allow for some variability between the pre- and post-aging values. Post-aging values exceeding this 30% window around the pre-aging values were of interest because it reflects the stimulation-induced changes in the values outside of the expected variability.

Comparisons of the electrochemical measurements throughout aging were only performed if there was a significant effect of aging. Since the conventional three-cell measurements could not be made throughout aging, the tripolar configuration used for delivering stimulation was also used for electrochemical

recordings. The recordings with this configuration were performed at day 7, 14, and 21.

Electrode surface characterization

On completion of the accelerated aging protocol, the surface condition of each electrode was evaluated for evidence of stimulus-induced damage including flaking of the electrode coating, pitting, corrosion, and surface deposits. The surface features of each electrode were examined using a FEI QUANTA 200 SEM. All electrodes were photographed at low ($\times 600$) and medium ($\times 2000$) magnification. A region of each electrode surface was then randomly selected and photographed at $\times 4000$ by a microscopist naïve to the experiment. The morphological changes to the appearance of the underlying Pt surface of the electrodes were defined by the extent of surface corrosion and was scored qualitatively on a scale of 0 (no corrosion) to 5 (severe corrosion) by a blinded, skilled observer (Shepherd *et al* 1985, 2018). The underlying Pt surface was visible under graphene electrodes and partially visible under Pt–Ir electrodes. A subset of the conductive hydrogel coated electrodes were imaged. Of the 22 conductive hydrogel coated electrodes scanned, 19 of them had sections of the underlying Pt visible. These sections were imaged and used for morphological corrosion analysis.

Trace analysis of Pt

The electrolyte in which each electrode array was chronically stimulated was analysed for trace levels of Pt using inductively coupled plasma mass spectrometry (ICP-MS) by the National Measurement Institute of the Australian Government (Shepherd *et al* 2019). Two samples were measured from each electrolyte sample using an Agilent 7700X ICP-MS system. Pt trace analysis was reported as the mean mass of Pt in mg/kg of electrolyte.

Statistical analysis

For all comparisons, Shapiro–Wilk was used to test normality and Brown–Forsythe tested the homogeneity of variance. $p \leq 0.05$ was used to indicate significance for all tests. Data are presented as median and quartiles unless otherwise stated.

The magnitude of the impedance from EIS, the CSC, VT impedance, and CIL before and after aging were compared using two-way analysis of variance (ANOVA) for main and interaction effects of the coating material and the aging process. All pairwise comparisons were performed using the Holm–Sidak method if the two-way ANOVA was significant.

Repeated measures ANOVA was used to compare the magnitude of the impedance from EIS, CSC, and VT impedance throughout aging. If tests for normality or equal variance failed, the Friedman repeated measures ANOVA on ranks was performed. Pairwise post hoc tests used the Holm–Sidak method if the repeated measures ANOVA was significant.

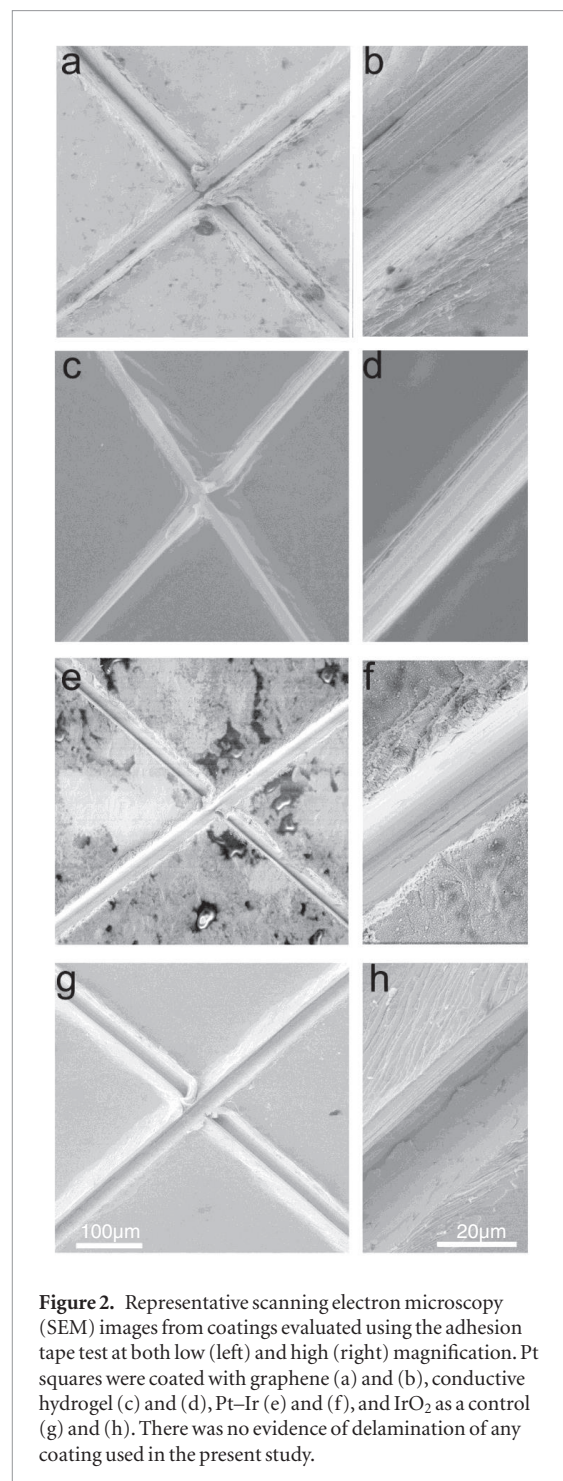


Figure 2. Representative scanning electron microscopy (SEM) images from coatings evaluated using the adhesion tape test at both low (left) and high (right) magnification. Pt squares were coated with graphene (a) and (b), conductive hydrogel (c) and (d), Pt–Ir (e) and (f), and IrO₂ as a control (g) and (h). There was no evidence of delamination of any coating used in the present study.

Analysis of the conductive hydrogel coated electrodes according to their Nyquist plot ‘type’ used the Mann–Whitney test to compare the pre-aging CSC and Kruskal–Wallis one-way ANOVA on ranks to compare the pre- and post-aging CSC and VT impedances.

The trace analysis of Pt was compared between materials using Kruskal–Wallis one-way ANOVA on ranks. Dunn’s method was used for pair-wise post hoc tests if ANOVA on ranks was significant.

The corrosion score of the electrodes of different charge densities was correlated with a line of best fit using linear regression. The extent of the corrosion of the electrodes and the quantity of the Pt particulates in

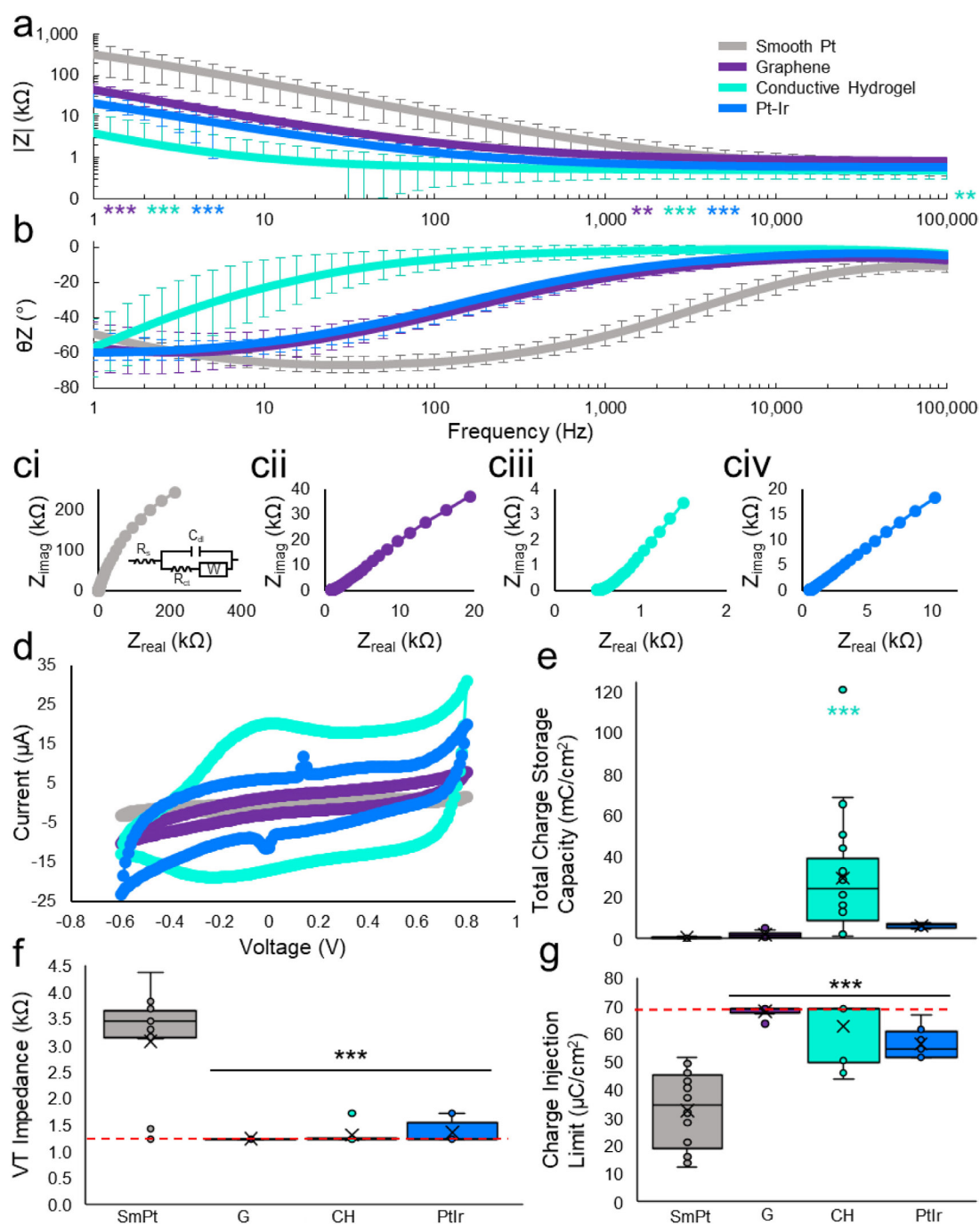


Figure 3. Electrochemical measurements using a three-cell configuration for each coating material prior to accelerated aging. (a) Mean (\pm standard deviation (SD)) magnitude of the impedance (Z) from electrical impedance spectroscopy (EIS) for all electrodes of each material. (b) Mean \pm standard deviation phase of the impedance from EIS for all electrodes of each material. (c) Mean Nyquist plots from EIS for (ci) smooth Pt, (cii) graphene, (ciii) conductive hydrogel, and (civ) Pt-Ir. Inset of (ci) general Randles model that describes the kinetics of the material-electrolyte interface. (d) Mean cyclic voltammograms (CV) for each material. (e) Median, interquartile range and 95% confidence limits for the total charge storage capacity (CSC) calculated from the area of the CV curves for each material. (f) Median, interquartile range, and 95% confidence limits for the voltage transient (VT) impedance for each coating material. The horizontal red dashed line at $1.23 \text{ k}\Omega$ represents the lowest possible impedance of the recording device. (g) Median, interquartile range, and 95% confidence limits for the charge injection limit (CIL) calculated from the VT for each material. The horizontal dashed line represents the highest possible charge injection limit ($69 \mu\text{C cm}^{-2}$), which corresponds to the current limit of 2 mA for the smallest electrode area. SmPt = smooth Pt; G = graphene; CH = conductive hydrogel. Z = impedance. In box and whiskers plots: \times = mean, \circ = raw data points. $**p \leq 0.01$; $***p \leq 0.001$. Asterisks indicating significance are colour-coordinated by material.

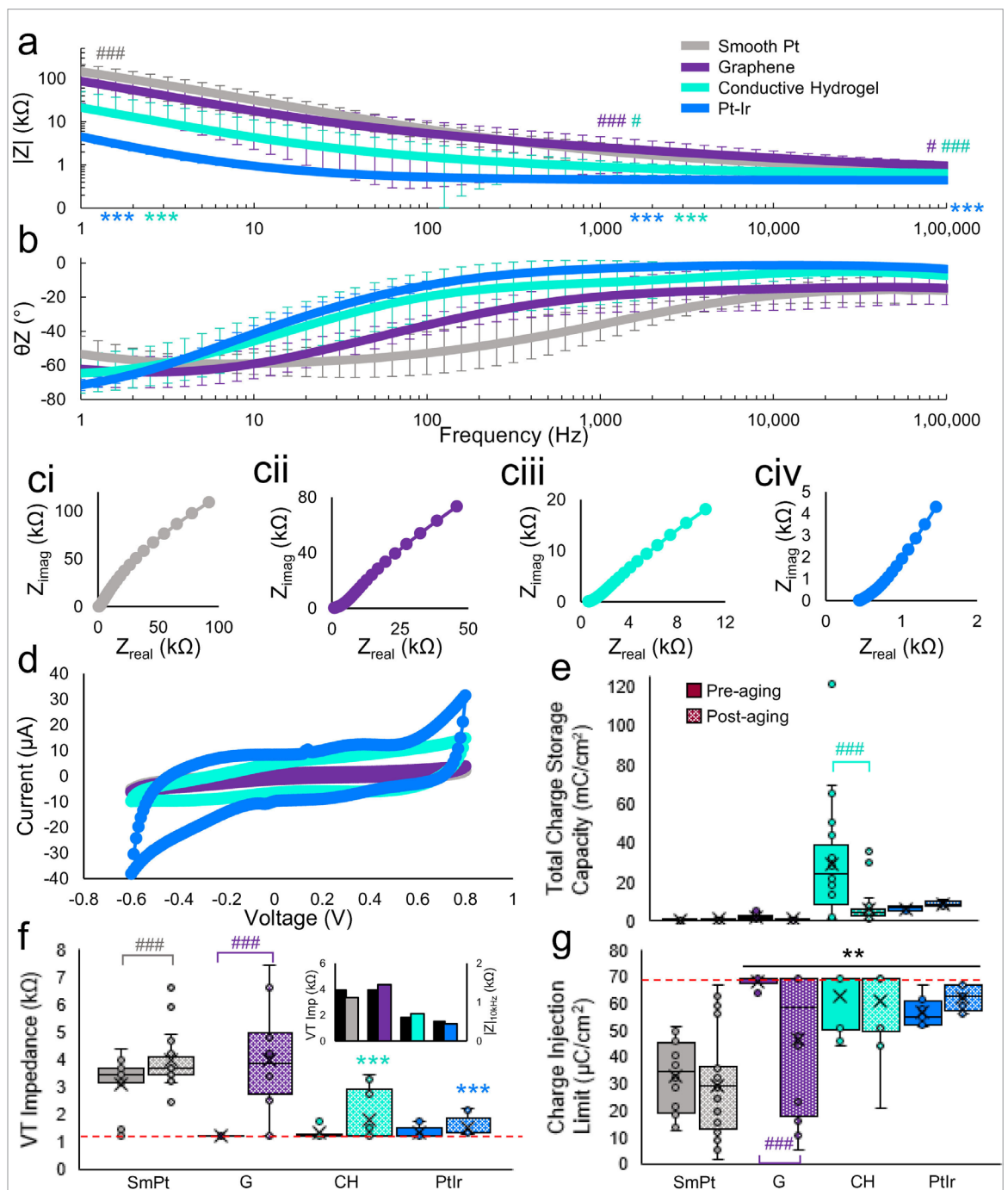
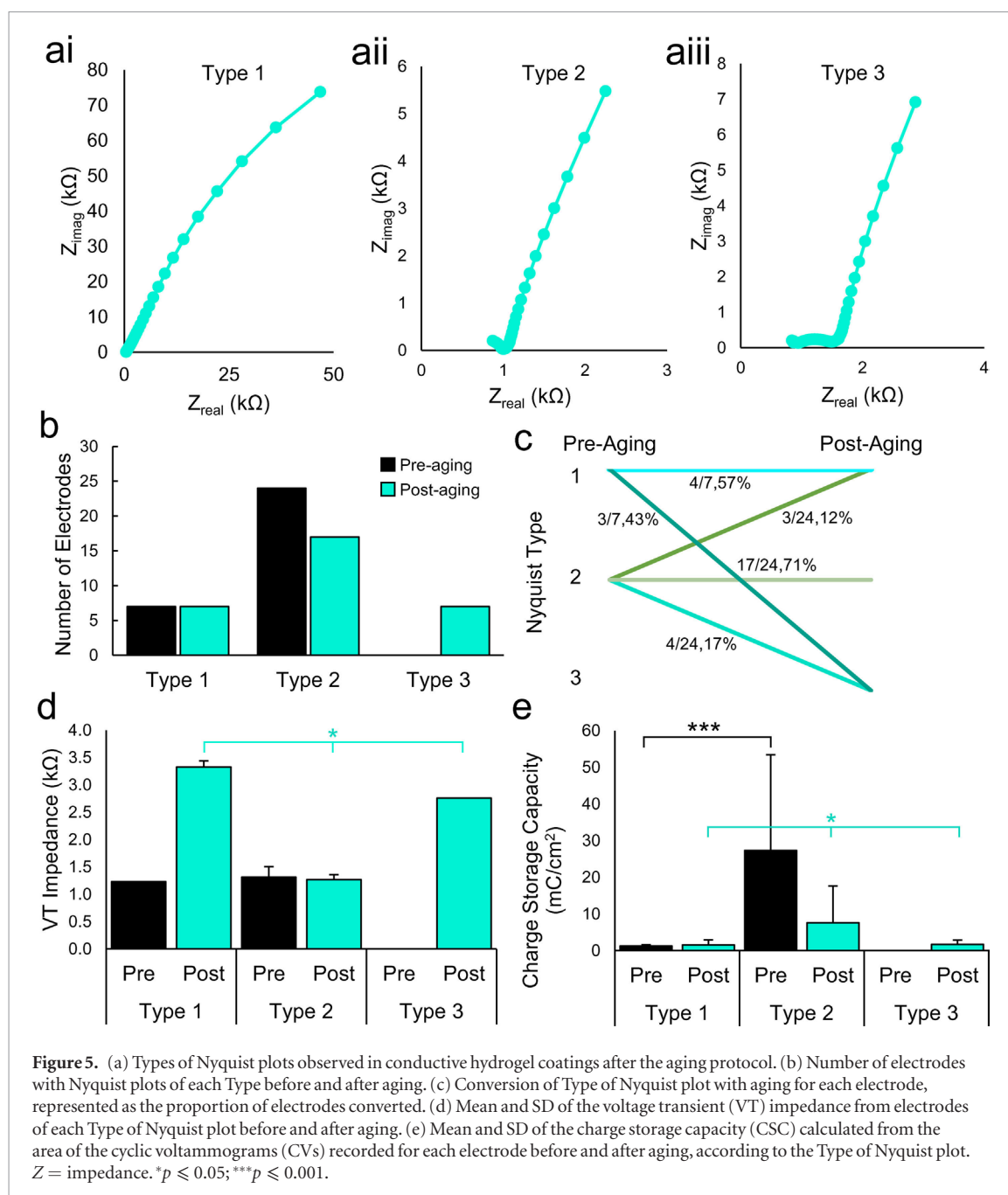


Figure 4. Electrochemical measurements using a three-cell configuration for each coating material after the 21 d accelerated aging protocol. (a) Mean (\pm SD) magnitude of the impedance from electrochemical impedance spectroscopy (EIS) for all electrodes of each coating material. (b) Mean \pm standard deviation phase of the impedance from EIS for all electrodes of each material. (c) Mean Nyquist plots from EIS for (c(i)) smooth Pt, (c(ii)) graphene, (c(iii)) conductive hydrogel, and (c(iv)) Pt-Ir. (d) Average cyclic voltammograms (CV) for each material. (e) Median, interquartile range and 95% confidence limits of the total charge storage capacity (CSC) for each material before (solid) and after (dotted) aging. (f) Median, interquartile range, and 95% confidence limits for the voltage transient (VT) impedance before (solid) and after (dotted) aging for each coating material. The horizontal red dashed line at 1.23 k Ω represents the lowest possible impedance of the recording device. Inset: average VT impedance (black) next to the average impedance magnitude from the EIS at 10 kHz (coloured). (g) Median, interquartile range, and 95% confidence limits for the charge injection limit (CIL) before (solid) and after (dotted) aging for each coating material. The horizontal dashed line represents the highest possible charge injection limit (69 $\mu\text{C cm}^{-2}$), which corresponds to the current limit of 2 mA for the smallest electrode area. SmPt = smooth Pt; G = graphene; CH = conductive hydrogel. Z = impedance. In box and whiskers plots: \times = mean, \circ = raw data points. * Indicates significant differences between materials; # indicates significant differences before and after aging. ** $p \leq 0.01$; *** $p \leq 0.001$; # $p \leq 0.05$; ## $p \leq 0.01$; ### $p \leq 0.001$. Symbols indicating significance are colour-coordinated by material.



the electrolyte were correlated using the Pearson Product-Moment correlation.

Results

Adhesion testing

The adhesion of the coatings was evaluated using at least three samples from each coating material as well as IrO₂ coated controls using the adhesion-by-tape test. SEM images revealed no evidence of delamination for any of the samples (figure 2). Some tape adhesive residue can be seen on samples coated with Pt-Ir (figure 2(e)). This is a common phenomenon for porous coatings that adhere well to the underlying surface. Tape residue following adhesion testing has been reported previously with sputtered iridium

oxide films (SIROF) coatings designed for a retinal prosthesis (Cogan *et al* 2004, 2009).

Electrochemical characterization of electrode materials

Comparing materials prior to aging

The coatings of graphene, conductive hydrogel, and Pt-Ir were compared with uncoated smooth Pt using standard electrochemical methods prior to the aging process. The Bode plots for each material represent the mean amplitude and phase of the impedance measured for all electrodes with that coating. The conductive hydrogel coating had a very low impedance magnitude throughout the entire frequency spectrum and was significantly lower than the impedance magnitude of smooth Pt at low, mid, and high frequencies

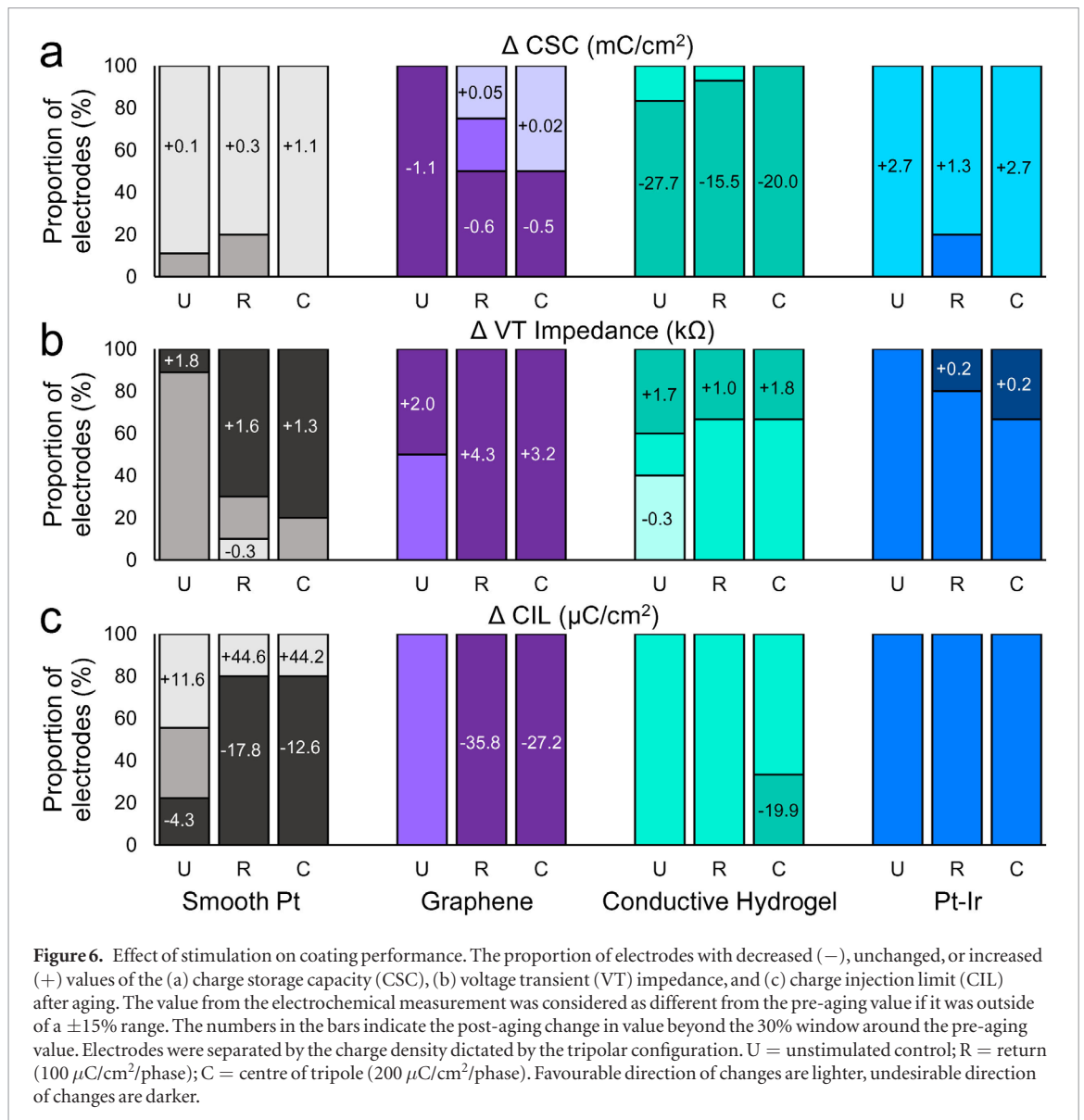


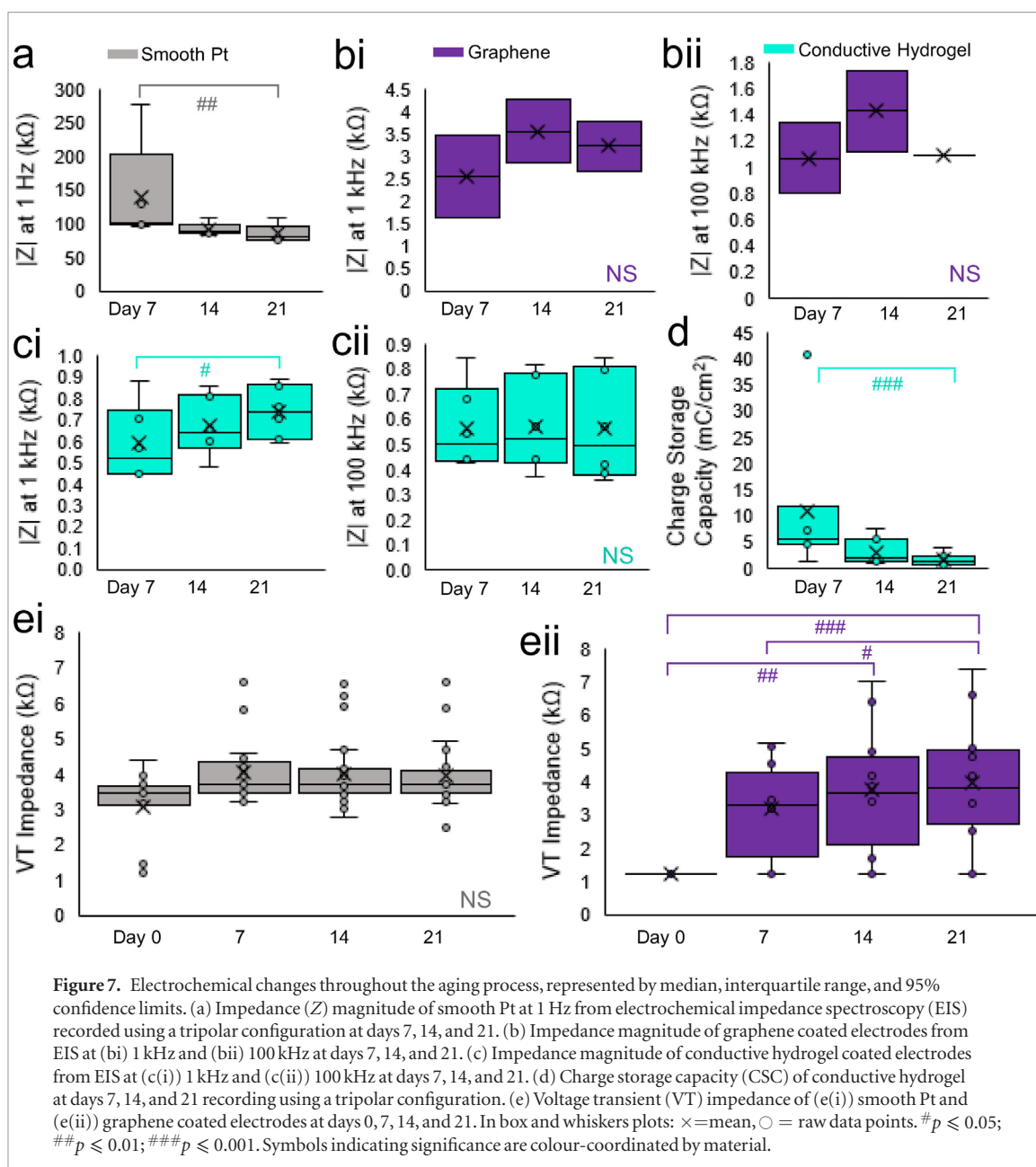
Figure 6. Effect of stimulation on coating performance. The proportion of electrodes with decreased (–), unchanged, or increased (+) values of the (a) charge storage capacity (CSC), (b) voltage transient (VT) impedance, and (c) charge injection limit (CIL) after aging. The value from the electrochemical measurement was considered as different from the pre-aging value if it was outside of a $\pm 15\%$ range. The numbers in the bars indicate the post-aging change in value beyond the 30% window around the pre-aging value. Electrodes were separated by the charge density dictated by the tripolar configuration. U = unstimulated control; R = return ($100 \mu\text{C}/\text{cm}^2/\text{phase}$); C = centre of tripole ($200 \mu\text{C}/\text{cm}^2/\text{phase}$). Favourable direction of changes are lighter, undesirable direction of changes are darker.

(1 Hz, 1 kHz, and 100 kHz; $p < 0.01$; figure 3(a)). The impedance magnitude of graphene and Pt–Ir coated electrodes was also significantly lower than smooth Pt at 1 Hz and 1 kHz ($p \leq 0.005$). The phase of the impedance for graphene, conductive hydrogel, and Pt–Ir coatings approached 0° at a much lower frequency than smooth Pt, with the phase for conductive hydrogel near 0° for almost the entire frequency spectrum (figure 3(b)). The shape of the Nyquist plots for all materials indicate a Randles equivalent circuit consisting of the electrolyte resistance in series with the parallel combination of the double-layer capacitance with the charge transfer resistance and Warburg impedance (figure 3(c)) (Randles 1947).

Cycles 2 to 10 from the CVs were used to generate a mean CV for each electrode. The means for each electrode were then averaged with the means from other electrodes of the same coating material to produce a representative CV curve (figure 3(d)). The CSC of graphene ($M_G = 1.6$; $Q1 = 0.3$; $Q3 = 2.5 \text{ mC}$

cm^{-2}) was not significantly different from the CSC of smooth Pt ($M_{\text{SPt}} = 0.5$; $Q1 = 0.3$; $Q3 = 0.8 \text{ mC cm}^{-2}$; $p = 0.736$). Pt–Ir also did not have a significantly different CSC ($M_{\text{Pt-Ir}} = 6.7$; $Q1 = 5.2$; $Q3 = 7.2 \text{ mC cm}^{-2}$) compared with smooth Pt ($p = 0.548$). Conductive hydrogel had the largest CSC ($M_{\text{CH}} = 24.4$; $Q1 = 8.8$; $Q3 = 38.9 \text{ mC cm}^{-2}$), which was significantly higher than the smooth Pt CSC ($p < 0.001$) but with high variability (figure 3(e)).

VT impedances and CILs were measured for all electrodes on all arrays except for 1 cochlear array that was coated with conductive hydrogel. Each coating had a significantly lower VT impedance compared with smooth Pt ($M_{\text{SPt}} = 3.5$; $Q1 = 3.1$; $Q3 = 3.6$; $p < 0.001$; figure 3(f)). The lowest possible VT impedance value was $1.23 \text{ k}\Omega$ due to the internal resistance of the recording device. All graphene coated electrodes had a VT impedance value at this lower limit. Additionally, 11 of the 14 conductive hydrogel coated electrodes ($M_{\text{CH}} = 1.23$; $Q1 = 1.23$; $Q3 = 1.24$), 6 of the



9 Pt–Ir coated electrodes ($M_{\text{Pt-Ir}} = 1.23$; $Q1 = 1.23$; $Q3 = 1.53$), and 2 of the 24 smooth Pt electrodes had VT impedance values at this lower limit.

Each coating had a significantly higher CIL compared with smooth Pt ($M_{\text{SPt}} = 34.5$; $Q1 = 18.9$; $Q3 = 45.2$; $p < 0.001$; figure 3(g)). The upper limit for the CIL was $69 \mu\text{C cm}^{-2}$, which corresponds to the current limit of 2 mA for the smallest electrode area. Nine of 12 graphene coated electrodes ($M_{\text{G}} = 69.0$; $Q1 = 67.6$; $Q3 = 69.0$) and 10 of 14 conductive hydrogel coated electrodes ($M_{\text{CH}} = 69.0$; $Q1 = 49.9$; $Q3 = 69.0$) reached the upper limit of the CIL.

Accelerated aging effects

An important consideration for coating materials on a neural interface is consistency throughout the implantation period. The aging process used in the present study was designed to simulate 1.6 years of

use to reveal the reliability of the coatings under active conditions *in vitro*.

Bode plots revealed that, after accelerated aging, the Pt–Ir coating had the lowest impedance magnitude, which was significantly lower than the impedance for smooth Pt (1 Hz, 1 kHz, and 100 kHz; $p \leq 0.001$; figure 4(a)). The low-frequency (1 Hz) impedance for smooth Pt significantly decreased after aging ($p < 0.001$). The impedance magnitudes of graphene and conductive hydrogel coatings at 1 kHz and 100 kHz significantly increased after aging ($p < 0.05$). However, the conductive hydrogel still had a significantly lower impedance magnitude than smooth Pt at 1 Hz and 1 kHz after aging ($p < 0.001$). Additionally, the average phase of the impedance for conductive hydrogel did not approach 0° as quickly as it did before the aging protocol, but approached 0° similarly to Pt–Ir (figure 4(b)).

After accelerated aging, Pt–Ir had the largest CSC ($M_{\text{Pt-Ir}} = 8.7$; $Q1 = 7.8$; $Q3 = 9.2 \text{ mC cm}^{-2}$; figures 4(d)–(e)), but it was not significantly different from the CSC for smooth Pt ($M_{\text{SPt}} = 0.8$; $Q1 = 0.6$; $Q3 = 1.3 \text{ mC cm}^{-2}$; $p = 0.466$). The CSC for conductive hydrogel coated electrodes ($M_{\text{CH}} = 4.1$; $Q1 = 2.5$; $Q3 = 6.4 \text{ mC cm}^{-2}$) significantly decreased after aging ($p < 0.001$) and was not significantly different from the CSC for smooth Pt ($p = 0.449$). The CSC for graphene ($M_{\text{G}} = 0.9$; $Q1 = 0.7$; $Q3 = 1.4 \text{ mC cm}^{-2}$) was comparable to the CSC of smooth Pt ($p = 0.982$).

Both smooth Pt ($M_{\text{SPt}} = 3.7$; $Q1 = 3.5$; $Q3 = 4.1 \text{ k}\Omega$) and graphene coated ($M_{\text{G}} = 3.8$; $Q1 = 2.7$; $Q3 = 4.9 \text{ k}\Omega$) electrodes exhibited a significant increase in VT impedance after accelerated aging ($p \leq 0.001$; figure 4(f)). Electrodes coated with conductive hydrogel ($M_{\text{CH}} = 1.2$; $Q1 = 1.2$; $Q3 = 2.9$) and Pt–Ir ($M_{\text{Pt-Ir}} = 1.3$; $Q1 = 1.3$; $Q3 = 1.8$) had a significantly lower VT impedance than smooth Pt electrodes ($p < 0.001$), with half of the conductive hydrogel coated electrodes at the lower impedance limit of $1.23 \text{ k}\Omega$. The VT impedance and the magnitude of the impedance from EIS at 10 kHz had similar relationships across materials (figure 4(f) inset).

All electrode coating materials had a significantly higher CIL than smooth Pt after aging ($p < 0.005$), despite the variability and significant decrease in the CIL for graphene coated electrodes ($p < 0.001$; figure 4(g)). All Pt–Ir coated electrodes and all except one conductive hydrogel coated electrode reached the upper polarization limit, with the variation due to the geometric area of the electrodes.

Variation in conductive hydrogel coating

After the accelerated aging protocol, a variety of shapes of Nyquist plots were observed for the conductive hydrogel coated electrodes and were divided into three categories (figure 5(a)). Type 1 was similar in shape to the Nyquist plots observed for all other electrodes in the present study and implies an extremely high charge transfer resistance, typical of blocking materials such as Pt that are dominated by the double-layer capacitance (Duan *et al* 2004, Lu *et al* 2010, Alba *et al* 2015). The second type of Nyquist plot observed was stereotypical of most of the conductive hydrogel coated electrodes prior to aging (figure 5(b)). It had a low charge transfer resistance compared with the model in Type 1, as well as low values for the double-layer capacitance and contribution from diffusion. The third type of Nyquist plot was only observed in 7/31 conductive hydrogel coated electrodes after the aging process and was present for both disc and ring electrodes. These electrodes were categorized as Type 1 or 2 electrodes prior to aging, but as Type 3 after aging (figure 5(c)). A Type 3 Nyquist plot suggests a larger contribution from the double-layer capacitance and small charge transfer resistance (Alba *et al* 2015). Prior to aging, all electrodes (both Type 1 and Type 2) had a low VT impedance (figure 5(d)), but the electrodes exhibiting

Type 1 behaviour had a significantly lower CSC than the Type 2 electrodes ($p < 0.001$; figure 5(e)). Interestingly, after aging, the Type 1 and Type 3 electrodes had a significantly higher VT impedance ($p \leq 0.02$) and significantly lower CSC than the Type 2 electrodes ($p < 0.02$). These results imply not only a change in kinetics after aging, but variability within the kinetics of the coatings.

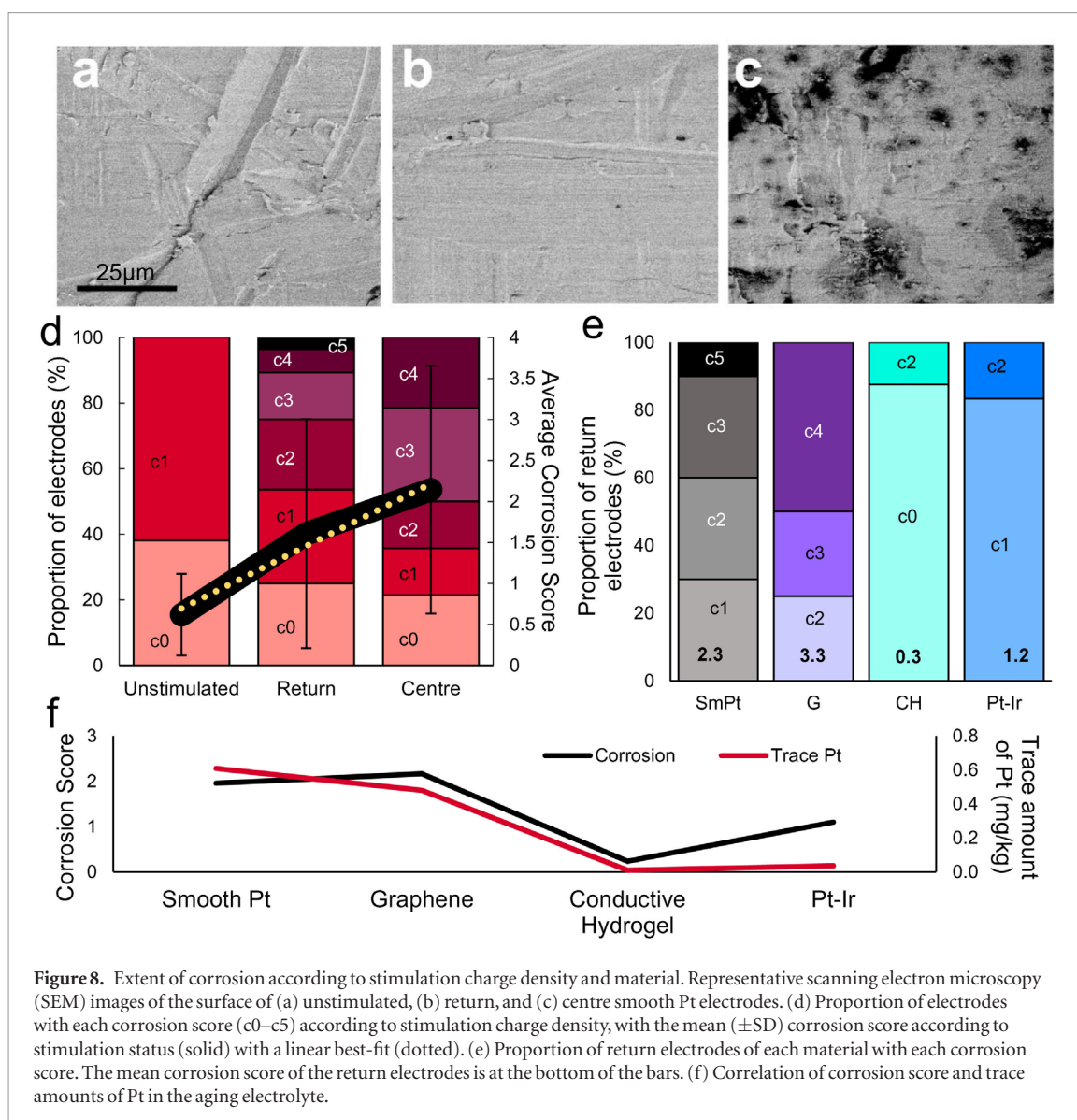
Effect of stimulation

With the tripolar stimulation configuration used to deliver stimulation throughout aging, electrodes developed one of three levels of charge density. The electrode at the centre of the tripole developed a charge density of $200 \mu\text{C}/\text{cm}^2/\text{phase}$; the return electrodes developed a charge density of $\sim 100 \mu\text{C}/\text{cm}^2/\text{phase}$; and the other electrodes served as unstimulated controls. If the post-aging electrochemical measurement changed by 15% or more from the pre-aging value (30% window), it was labelled as having a different value from the baseline and the magnitude of the difference between pre- and post-aging was computed (figure 6).

The CSC of most smooth Pt electrodes increased after aging, regardless of the charge density developed at the electrode. However, a larger proportion of smooth Pt centre and return electrodes had an increase in VT impedance (up to $1.6 \text{ k}\Omega$ above the 30% window) and a decrease in CIL (up to $17.8 \mu\text{C cm}^{-2}$ below the 30% window) after aging, reducing the effectiveness of these electrodes. Similarly, graphene coated electrodes displayed a reduced CSC in half of all return and centre electrodes (up to 0.6 mC cm^{-2} below the 30% window), and a higher VT impedance (up to $4.3 \text{ k}\Omega$ above the 30% window) and much lower CIL (up to $35.8 \mu\text{C cm}^{-2}$ below the 30% window) in all return and centre electrodes, suggesting a strong effect from the stimulation on the coating. Electrodes coated with conductive hydrogel typically had large reductions in CSC (up to 27.7 mC cm^{-2} below the 30% window) regardless of whether or not the electrode was stimulated. The unstimulated conductive hydrogel coated electrodes had an increased, unchanged, and decreased VT impedance (40%, 20%, 40%, respectively), with a small proportion of the stimulated electrodes increasing in impedance with aging. They exhibited little change in CIL, with a small proportion of centre electrodes having a decrease in CIL. Generally, the Pt–Ir electrodes remained unchanged with aging, with some evidence of an increase in the CSC across all electrodes. A possible stimulation effect was evident on the VT impedance, with a small ($0.2 \text{ k}\Omega$ above the 30% window) proportion of electrodes increasing in the VT impedance with aging. The CIL after aging did not exceed the 30% window around pre-aging values for any electrode electrodeposited with Pt–Ir.

Electrochemical changes throughout aging

If a significant difference between the pre-aging and post-aging measures was found, repeated measures



were performed to include days 7 and 14 of the aging protocol. As noted above, these recordings were performed using the tripolar configuration, as opposed to the standard 3-cell configuration. The change in magnitude of the impedance at 1 Hz for smooth Pt was significant between days 7 and 21 ($p = 0.004$; figure 7(a)). Although there were significant differences between the impedance magnitudes for graphene coatings at 1 kHz and 100 kHz, there were no significant differences between days 7 and 21 ($p_{1 \text{ kHz}} = 0.167$; $p_{100 \text{ kHz}} = 0.5$; figures 7(b(i) and (ii))). The change in magnitude of the impedance at 1 kHz for conductive hydrogel was significant between days 7 and 21 ($p = 0.012$), but no difference was found at 100 kHz ($p = 0.923$; figures 7(c(i) and (ii))). These results suggest that for graphene, changes in the magnitude of the impedance likely occur within the first week and were therefore not captured in these repeated measures. There were no significant changes in the electrochemical measures for Pt–Ir coated electrodes after aging compared to before aging; therefore, repeated measures were not performed for this group.

The CSC of conductive hydrogel coatings differed significantly between 7 and 21 days only ($p < 0.001$), suggesting subtle changes each week that are eventually significant (figure 7(d)). Smooth Pt and graphene coated electrodes had significant differences in their VT impedances after aging. A significant difference was not found for smooth Pt electrodes throughout aging ($p = 0.076$; figure 7(e(i))). Graphene coated electrodes at 14 and 21 days into the aging process had VT impedances that were significantly higher than the pre-aging impedance ($p \leq 0.003$), with significant differences between days 7 and 21 also found ($p = 0.023$). This suggests continual changes to the VT impedance of graphene coated electrodes throughout the aging process.

Surface properties of electrodes

The extent of surface corrosion was optically characterized by grading on a scale from 0 to 5 by a blinded observer, naïve to the stimulation status of the electrodes. Varying extents of corrosion were observed for the unstimulated, return, and centre electrodes

Table 2. Trace analysis of Pt from the electrolyte that contained the arrays during the aging process. Two samples of electrolyte were processed for each array.

Electrode coating	Electrode array ID	Trace analysis of Platinum (mg kg^{-1})	
		Sample 1	Sample 2
Smooth Pt	SPt_01	0.86	0.90
	SPt_02	0.52	0.54
	SPt_03	0.44	0.45
	SPt_04	0.50	0.51
	SPt_05	0.69	0.68
Reduced graphene oxide	GR_01	0.41	0.42
	GR_02	0.55	0.54
Conductive hydrogel ^a	CH_01	<0.01	<0.01
	CH_02	<0.01	<0.01
	CH_03	<0.01	<0.01
	CH_04	<0.01	<0.01
Electrodeposited Pt–Ir ^a	PtIr_01	<0.01	<0.01
	PtIr_02	0.027	0.032
	PtIr_03	0.066	0.069

^a Compared with smooth Pt; $p < 0.05$.

(figure 8(a)). As expected, the extent of the corrosion increased with the charge density at the electrode, with a strong linear correlation (figure 8(b); $R^2 = 0.97$). Further analysis of the return electrodes separated by material revealed that graphene coated electrodes had high levels of corrosion, with an average corrosion score higher than that of smooth Pt (smooth Pt: 2.3; graphene: 3.3). Conductive hydrogel (0.3) and Pt–Ir (1.2) return electrodes showed very little corrosion of the underlying Pt (figure 8(c)).

Trace analysis of Pt

Trace analysis for Pt in the electrolyte samples revealed that smooth Pt electrodes had significantly higher amounts of Pt than the electrolyte samples from conductive hydrogel and Pt–Ir coatings ($p < 0.03$; table 2). Electrolyte samples from graphene coated electrodes had comparable levels of Pt to the samples from smooth Pt electrodes ($p = 1.0$). The extent of corrosion and trace amounts of Pt found in the electrolyte were strongly correlated ($R^2 = 0.895$; figure 8(d)).

Discussion

Three materials—reduced graphene oxide, conductive hydrogel, and electrodeposited Pt–Ir—were coated onto ring and disc Pt electrodes. These materials were compared with smooth Pt electrodes using mechanical and electrochemical tests throughout a 21 d accelerated aging protocol with an equivalence to 1.6 years of use. This accelerated aging timeframe allowed for a screening of the materials for further testing *in vivo*.

Mechanical evaluation of the coatings was done using the adhesion-by-tape test and by characterizing the electrode surface after aging. All coating materials adhered well to the smooth Pt, as none of the coatings delaminated. The effect of accelerated aging through continuous electrical stimulation on the integrity of the coating and underlying Pt was evaluated by examining the electrode surface for corrosion. Corrosion scores and the trace amount of Pt in the electrolyte were strongly correlated, indicating that the corrosion led to trace amounts of Pt accumulating in the electrolyte. Both conductive hydrogel and Pt–Ir had significantly lower levels of Pt in the electrolyte when compared with smooth Pt, with graphene having similar Pt levels as smooth Pt. Corrosion of Pt is undesirable as it can reduce the lifetime of the implant and recent *in vitro* studies have shown that at high concentrations of Pt ions can induce cell death (Wissel *et al* 2018).

Electrochemical evaluation of the materials was achieved using several measures. EIS enables the investigation of the impedance over a wide range of frequencies. Reactions at the electrode–electrolyte interface define the impedance magnitude over different ranges of the frequency spectra. For example, at high frequencies, the impedance is dominated by the electrolyte resistance, with a phase very close to 0° (Cogan 2008). Therefore, the impedances of all materials at 100 kHz prior to aging were very low and similar in magnitude, with a phase near 0° . The impedance at low frequencies is dominated by a constant phase element, likely a double-layer capacitor, as the phase of the impedance nears 90° . It is favourable if the impedance magnitude approaches the solution resistance and the phase angle approaches 0° at as low a frequency as possible, as this indicates that the interface has minimal accumulation of charge, i.e. electrode polarization. All three coatings were favourable over smooth Pt, with conductive hydrogel approaching the solution resistance and 0° phase at lower frequencies than graphene and Pt–Ir prior to aging. However, after the aging protocol, the impedance for Pt–Ir approached the solution resistance and 0° phase at lower frequencies than all other materials, i.e. almost no electrode polarization was observed. This decrease in impedance of Pt–Ir after stimulation is similar to the results of previous studies of electrodes containing Ir, in which repeated cyclic voltammetry and/or stimulation caused the formation of activated IrO_2 and a decrease in the impedance of the electrode (Beebe and Rose 1988, Troyk *et al* 2004). The phase of the impedance for conductive hydrogel coated electrodes still approached 0° at low frequencies and the magnitude of the impedance increased but remained close to the solution resistance over the frequency spectra. Since the conductive hydrogel and Pt–Ir coatings had an impedance magnitude that approached the solution resistance across the frequency range, they may provide a more consistent delivery of non-polarizing charge during use.

The impedance spectra for graphene were similar to smooth Pt after aging.

CV curves were used to calculate CSC, which represents the total area of the electrode and its ability to pass charge at low frequencies. Conductive hydrogel electrodes had a significantly larger CSC before aging compared with smooth Pt, while Pt–Ir electrodes had a greater CSC after aging, irrespective of the charge density developed at that electrode. Nearly all conductive hydrogel coated electrodes, regardless of the charge density, had a large decrease in the CSC throughout aging, paired with a reduction in the variability in the CSC. A drop in the electrochemical charge transfer properties of conductive hydrogel materials and also conductive polymer based materials more generally is expected. It has been shown that these materials undergo chain rearrangements and loss of doping components over the initial period of use. This drop in CSC is known to plateau to yield stable electrochemical characteristics in the long-term (Yamato 1995, Cui *et al* 2003, Green *et al* 2012b, 2013, Goding *et al* 2017a, Staples *et al* 2017). Interestingly, a large proportion of the stimulated smooth Pt and graphene coated electrodes exhibited an increase in CSC. This may be due to pitting caused by corrosion, which would increase the effective surface area of those electrodes (Green *et al* 2014).

Also of note, the CV curves recorded from the Pt–Ir coated electrodes had distinct oxidation and reduction peak pairs at approximately 140 mV (on the oxidation sweep) and -10 mV (on the reduction sweep) (figure 3(d)). These peaks were present in all electrodes prior to aging, but only in three of the nine electrodes after the aging process, with no relationship to the stimulation charge density at the electrodes. Since peaks occurred on both the oxidative (forward) scan and the reductive (reverse) scan and the ratio of the current at each peak was equal to one, the reactions were reversible (Chiku *et al* 2008). These peaks are similar to oxidation/reduction peaks associated with Ag (Van der Horst *et al* 2015) and may indicate surface contamination. After aging the peaks are reduced or absent. This may be due to the contaminate being removed during the aging process.

Both Pt and Ir have characteristic oxidation peaks and shoulders associated with the transition of Pt and Ir through various different oxidation states (Tremiliosi-Filho 1991, Burke 1993). As Pt and Ir progressively oxidize and reduce in the PBS solution, they form disorganized oxides on the electrode surface. This can lead to changes in the total surface area as well as remodelling of the electrode topology. This reorganization could lead to shielding/blocking of exposed non-Pt–Ir metallic sites, and thus cause the anomalous peaks to decrease.

EIS can also produce Nyquist plots, which represent the real and imaginary components of the impedance throughout the frequency spectra. The shape of

the Nyquist plot and the values from the magnitude and phase of the impedance can be used to model the electrode-electrolyte interface. The data from all materials suggest a Randles cell model (Randles 1947); the values of the components of the model were not calculated, as those specifics were beyond the scope of this work. However, three noticeably different shapes of Nyquist plots were observed for the conductive hydrogel coated electrodes after aging, each with unique electrochemical properties. By approximating the values of the Randles model according to the types of Nyquist plots observed (figure 5), the mechanisms behind these changes over time can be inferred. The distinct shapes of the Nyquist plots may indicate differences in the quality of the coating. Prior to aging, some of the conductive hydrogel coated electrodes exhibited Type 1 Nyquist plot characteristics that are similar in shape to smooth-Pt coated electrodes. These electrodes also had a smaller CSC than those belonging to a Type 2 Nyquist plot. It is possible that the coating of these electrodes may have been inadequate or that the coating did not have intimate contact with the Pt surface. The electrodes exhibiting a Type 2 Nyquist plot, which is stereotypical of polymer coated electrodes (Alba *et al* 2015), had variable CSC which may suggest variability in the amount of conductive hydrogel coated onto each electrode. After aging, a number of Type 2 conductive hydrogel electrodes changed to Type 1 or Type 3 Nyquist shapes. These changes were paired with a significant increase in the VT impedance and decrease in the CSC. Similar changes in the presence of a semi-circular arc have been shown to occur *in vivo*, corresponding to increased tissue encapsulation (Alba *et al* 2015). As there was no tissue to encapsulate the electrodes in this study, this may instead indicate the possibility that the coatings were not fully intact or delaminated after aging. In fact, there were sections on some of the conductive hydrogel coated electrodes where the underlying Pt was visible, which enabled surface corrosion analysis. Although the electrochemical changes occurred in only a small number of electrodes, it will be important to closely monitor this behaviour in future *in vivo* studies.

The impedance magnitude at 1 kHz is often reported and used to compare different materials developed for neural interfaces because it is related to the duration of an action potential in neurons (Mercanzini *et al* 2009). This may be more relevant to recording electrodes. However, for stimulation applications a 1 kHz frequency corresponds to a pulse width of 1 ms, which is very long for most applications in medical bionics, excluding retinal prostheses (Cogan 2008). An additional measure of impedance using a VT with a pulse width of 100 μ s, which is a common clinical value and corresponds to a frequency of 10 kHz, was used (Zeng *et al* 2008). The maximum VT at the shorter pulse widths are more relevant for constant-current stimulators, which are commonly used, as the

maximum VT is important in determining the voltage compliance of the stimulator (Seligman 2009). As expected, the VT impedance and the magnitude of the impedance at 10 kHz had similar relationships for all materials, demonstrating consistent results between the two methods. Both conductive hydrogel and Pt–Ir coatings maintained a significantly lower VT impedance after aging, even in the stimulated electrodes. As noted in the results, the recording equipment was limited to a lower limit of 1.23 k Ω , so it is very possible that the VT impedances of these coatings were even lower than 1.23 k Ω . Graphene coated electrodes demonstrated a steady increase in impedance throughout the aging period. Maintaining a low impedance is a requirement for electrode coatings as it allows for safe charge injection.

Before and after aging, all coating materials had a higher CIL than smooth Pt, often reaching the upper limit of 2 mA, which corresponds to a maximum of 69 $\mu\text{C cm}^{-2}$ for the smallest electrodes used in the present study. Every electrode coated with Pt–Ir and all but one coated with conductive hydrogel reached the upper limit, with the variability in CIL due to the variability in the size of the electrodes used. Although graphene coated electrodes also had a significantly higher CIL than smooth Pt, there was a wide range in CIL values, regardless of electrode area. When considering only the electrodes that were stimulated, all graphene coated electrodes presented with a very large decrease in CIL over the aging period. Alongside an increased impedance and reduced CSC that also disproportionately affect stimulated electrodes, graphene coated electrodes did not present a substantial advantage over smooth Pt electrodes after aging. Both the conductive hydrogel and Pt–Ir had a larger CSC, significantly lower impedance, and significantly higher CIL both before and after aging. However, the conductive hydrogel electrodes had more variability in their electrochemical properties with the aging process.

The aging protocol implemented in this study tested the reliability and integrity of the electrode coatings under challenging conditions including high temperatures and continuous stimulation at a very high stimulation charge density. A stimulation charge density of 200 $\mu\text{C/cm}^2/\text{phase}$ has been previously shown to corrode smooth Pt electrodes *in vivo* (Shepherd *et al* 2019). As a comparison, a typical moderate stimulation charge density for cochlear implant users is approximately 9 $\mu\text{C/cm}^2/\text{phase}$. Although the materials may not perform optimally under these conditions, enduring the aging protocol served as a rigorous screening criterion for the coatings. Chronic *in vivo* testing is required to further determine the effectiveness of the conductive hydrogel and Pt–Ir coatings, both mechanically and electrochemically, in a more challenging and realistic environment. If these coating materials remain effective and stable *in vivo* chroni-

cally, they would have potential application in many bionic devices including cochlear implants, electrocorticography, and deep brain and spinal cord stimulators. Several conductive coatings are currently under development for various applications, including glassy carbon or porous graphene on flat disc electrodes for electrocorticography over the somatosensory cortex (Nimbalkar *et al* 2018, Vomero *et al* 2018) or PEDOT variants on small surface area tips of sharp penetrating electrodes implanted in the brain for deep brain stimulation (Bodart *et al* 2019) and in the spinal cord for intraspinal microstimulation (Vara and Collazos-Castro 2019). Therefore, conductive coatings are a viable option for the improving electrochemical performance of electrodes for a variety of neuroprosthetic applications. Incorporation of conductive coatings onto softening substrates, such as those made with thiolene (Arreaga-Salas *et al* 2015), may improve both electrical and mechanical performance of the electrodes.

Translation of conductive coatings to commercially available devices would not require extensive revision to manufacturing processes as they can be coated directly onto existing Pt electrodes. However, quality control during the coating process will have to be maintained to ensure reproducible and consistent coating quality. Care was taken in this study to ensure that the coating of the electrode arrays was done in a single batch. However, further improvements to the fabrication process may help reduce the variability observed in the coatings.

Conclusion

The goal of this study was to compare three candidate electrode coatings—reduced graphene oxide, conductive hydrogel, and electrodeposited Pt–Ir after a 21 d accelerated aging protocol. All three coating materials exhibited an electrochemical advantage over smooth Pt electrodes prior to aging. After aging, graphene coated electrodes displayed a stimulation-induced increase in impedance and reductions in charge storage capacity and charge injection limit, along with high levels of Pt corrosion and dissolution, resulting in no benefit over smooth Pt. Conductive hydrogel and Pt–Ir coated electrodes endured the aging process, with little corrosion, large charge storage capacity and charge injection limit, and low impedances compared to smooth Pt. Conductive hydrogel and Pt–Ir therefore represent excellent candidates for *in vivo* testing with potential use in future medical bionics devices.

Acknowledgments

This work was funded by the NHMRC of the Australian Government (APP1122055) and the Garnett Passe

and Rodney Williams Memorial Foundation for which we are most grateful. The Bionics Institute acknowledges support of the Victorian Government through Operational Infrastructure Support Program. We thank Dr A Thompson, C McGowan, V Maxim, H Feng, J Zhou, and R Thomas from the Bionics Institute, R Curtain and the SEM Facility at Bio21, the University of Melbourne for their excellent technical assistance, and staff at the National Measurement Institute of the Australian Government for ICP-MS analysis. We also thank Dr S Cogan and EIC Laboratories Inc. (USA) for providing us with the IrO₂ samples. Platinum Group Coatings (PGC) acknowledges the support of the Pasadena Bioscience Collaborative and thank J Sharkey and G Weiland for preparing test samples. We also thank Dr P Carter from Cochlear Ltd. for his valuable input on the manuscript.

Conflicts of interest

Curtis Lee, Artin Petrossians, John Whalen are employed by Platinum Group Coatings (PGC), which provided the electrodeposited Pt-Ir coatings. Artin Petrossians and John Whalen are also part owners of PGC. The remaining authors declare no financial interest in any material evaluated in the present study.

ORCID iDs

Ashley N Dalrymple  <https://orcid.org/0000-0001-8566-7178>

Ulises Aregueta Robles  <https://orcid.org/0000-0001-9162-465X>

John S Forsythe  <https://orcid.org/0000-0003-2849-229X>

Robert K Shepherd  <https://orcid.org/0000-0002-4239-3362>

James B Fallon  <https://orcid.org/0000-0003-2686-3886>

References

- Abbott C J et al 2018 Safety studies for a 44-channel suprachoroidal retinal prosthesis: a chronic passive study *Invest. Ophthalmol. Vis. Sci.* **59** 1410–24
- Alba N A, Du Z J, Catt K A, Kozai T D and Cui X T 2015 *In vivo* electrochemical analysis of a PEDOT/MWCNT neural electrode coating *Biosensors* **5** 618–46
- Amon A and Alesch F 2017 Systems for deep brain stimulation: review of technical features *J. Neural Trans.* **124** 1083–91
- ANSI 2017 Cochlear implant systems: requirements for safety, functional verification, labeling and reliability reporting ANSI/AAMI CI86:2017 (Arlington, VA: AAMI)
- Arreaga-Salas D E, Avendano-Bolivar A, Simon D, Reit R, Garcia-Sandoval A, Rennaker R L and Voit W 2015 Integration of high-charge-injection-capacity electrodes onto polymer softening neural interfaces *ACS Appl. Mater. Interfaces* **7** 26614–23
- ASTM 1997 *Standard Test Methods for Measuring Adhesion by Tape Test* (West Conshohocken, PA: ASTM International)
- ASTM 2011 *Standard Guide for Accelerated Aging of Sterile Barrier Systems for Medical Devices* (West Conshohocken, PA: ASTM International)
- Barolat G, Oakley J C, Law J D, North R B, Ketcik B and Sharan A 2001 Epidural spinal cord stimulation with a multiple electrode paddle lead is effective in treating intractable low back pain *Neuromodulation* **4** 59–66
- Beebe X and Rose T L 1988 Charge injection limits of activated iridium oxide electrodes with 0.2 ms pulses in bicarbonate buffered saline *IEEE Trans. Biomed. Eng.* **35** 494–5
- Bennett J A, Agbere I B and Moesta M 2016 Complete coating of underlying Pt electrodes by electrochemical reduction of graphene oxide *Electrochim. Acta* **188** 111–9
- Bodart C, Rossetti N, Hagler J, Chevreau P, Chhin D, Soavi F, Schougaard S B, Amzica F and Cicoira F 2019 Electropolymerized poly(3,4-ethylenedioxythiophene) (PEDOT) coatings for implantable deep-brain-stimulating microelectrodes *ACS Appl. Mater. Interfaces* **11** 17226–33
- Boehler C, Oberueber F, Schlabach S, Stieglitz T and Asplund M 2017 Long-term stable adhesion for conducting polymers in biomedical applications: IrOx and nanostructured platinum solve the chronic challenge *ACS Appl. Mater. Interfaces* **9** 189–97
- Burgio P 1986 Safety considerations of cochlear implantation *Otolaryngol. Clin. North Am.* **19** 237–47 (PMID: 3754947)
- Burke C and Morrissey J A 1993 An investigation of some of the variables involved in the generation of an unusually reactive state of platinum *Electrochim. Acta* **38** 897–906
- Chang C W, Lo Y K, Gad P, Edgerton R and Liu W 2014 Design and fabrication of a multi-electrode array for spinal cord epidural stimulation *Conf. Proc. IEEE Eng. Med. Biol. Soc.* pp 6834–7
- Chiku M, Ivandini T A, Kamiya A, Fujishima A and Einaga Y 2008 Direct electrochemical oxidation of proteins at conductive diamond electrodes *J. Electroanal. Chem.* **612** 201–7
- Clark G 2003 *Cochlear Implants: Fundamentals and Applications* (New York: Springer) (<https://doi.org/10.1063/1.1839383>)
- Cogan S F 2008 Neural stimulation and recording electrodes *Annu. Rev. Biomed. Eng.* **10** 275–309
- Cogan S F, Ehrlich J, Plante T D, Smirnov A, Shire D B, Gingerich M and Rizzo J F 2009 Sputtered iridium oxide films for neural stimulation electrodes *J. Biomed. Mater. Res. B* **89B** 353–61
- Cogan S F, Plante T D and Ehrlich J 2004 Sputtered iridium oxide films (SIROFs) for low-impedance neural stimulation and recording electrodes *Conf. Proc. IEEE Eng. Med. Biol. Soc.* **6** 4153–6
- Cui X, Wiler J, Dzaman M, Altschuler R A and Martin D C 2003 *In vivo* studies of polypyrrole/peptide coated neural probes *Biomaterials* **24** 777–87
- Duan Y Y, Clark G M and Cowan R S 2004 A study of intra-cochlear electrodes and tissue interface by electrochemical impedance methods *in vivo Biomaterials* **25** 3813–28
- Goding J, Gilmour A, Martens P, Poole-Warren L and Green R 2017a Interpenetrating conducting hydrogel materials for neural interfacing electrodes *Adv. Healthcare Mater.* **6** 1–13
- Goding J, Gilmour A, Robles U A, Poole-Warren L, Lovell N, Martens P and Green R 2017b A living electrode construct for incorporation of cells into bionic devices *MRS Commun.* **7** 487–95
- Green R A, Hassarati R T, bouchinet L, Lee C S, Cheong G L, Yu J F, Dodds C W, Suaning G J, Poole-Warren L A and Lovell N H 2012a Substrate dependent stability of conducting polymer coatings on medical electrodes *Biomaterials* **33** 5875–86
- Green R A, Hassarati R T, Goding J A, Baek S, Lovell N H, Martens P J and Poole-Warren L A 2012b Conductive hydrogels: mechanically robust hybrids for use as biomaterials *Macromol. Biosci.* **12** 494–501
- Green R A, Matteucci P B, Dodds C W, Palmer J, Dueck W F, Hassarati R T, Byrnes-Preston P J, Lovell N H and Suaning G J 2014 Laser patterning of platinum electrodes for safe neurostimulation *J. Neural Eng.* **11** 056017
- Green R A, Matteucci P B, Hassarati R T, Giraud B, Dodds C W, Chen S, Byrnes-Preston P J, Suaning G J, Poole-Warren L A and Lovell N H 2013 Performance of conducting polymer electrodes for stimulating neuroprosthetics *J. Neural Eng.* **10** 016009
- Green R and Abidian M R 2015 Conducting polymers for neural prosthetic and neural interface applications *Adv. Mater.* **27** 7620–37

- Hassarati R T, Dueck W F, Tasche C, Carter P M, Poole-Warren L A and Green R A 2014 Improving cochlear implant properties through conductive hydrogel coatings *IEEE Trans. Neural Syst. Rehabil. Eng.* **22** 411–8
- Hilder M, Winther-Jensen B, Li D, Forsyth M and Macfarlane D R 2011 Direct electro-deposition of graphene from aqueous suspensions *Phys. Chem. Chem. Phys.* **13** 9187–93
- Hukins D W, Mahomed A and Kukureka S N 2008 Accelerated aging for testing polymeric biomaterials and medical devices *Med. Eng. Phys.* **30** 1270–4
- Lee C D, Hudak E M, Whalen J J, Petrossians A and Weiland J D 2018 Low-impedance, high surface area Pt–Ir electrodeposited on cochlear implant electrodes *J. Electrochem. Soc.* **165** G3015–7
- Leung R T, Shivdasani M N, Nayagam D A and Shepherd R K 2015 *In vivo* and *in vitro* comparison of the charge injection capacity of platinum macroelectrodes *IEEE Trans. Biomed. Eng.* **62** 849–57
- Lu Y, Li T, Zhao X, Li M, Cao Y, Yang H and Duan Y Y 2010 Electrodeposited polypyrrole/carbon nanotubes composite films electrodes for neural interfaces *Biomaterials* **31** 5169–81
- Ludwig K A, langhals N B, Joseph M D, Richardson-Burns S M, Hendricks J L and Kipke D R 2011 Poly(3,4-ethylenedioxythiophene) (PEDOT) polymer coatings facilitate smaller neural recording electrodes *J. Neural Eng.* **8** 014001
- Mercanzini A, Colin P, Bensadoun J C, Bertsch A and Renaud P 2009 *In vivo* electrical impedance spectroscopy of tissue reaction to microelectrode arrays *IEEE Trans. Biomed. Eng.* **56** 1909–18
- Nimbalkar S, Castagnola E, Balasubramani A, Scarpellini A, Samejima S, Khorasani A, Boissenin A, Thongpang S, Moritz C and Kassegne S 2018 Ultra-capacitive carbon neural probe allows simultaneous long-term electrical stimulations and high-resolution neurotransmitter detection *Sci. Rep.* **8** 6958
- Ouyang L, Wei B, Kuo C C, Pathak S, Farrell B and Martin D C 2017 Enhanced PEDOT adhesion on solid substrates with electrografted P(EDOT-NH₂) *Sci. Adv.* **3** e1600448
- Patrick J F, Seiigman P M, Money D K and Kuzma J A 1990 *Engineering Cochlear Prostheses* ed G Clark et al (Edinburgh: Churchill Livingstone)
- Petrossians A, Whalen J J, Weiland J D and Mansfeld F 2011a Electrodeposition and characterization of thin-film platinum-iridium alloys for biological interfaces *J. Electrochem. Soc.* **158** D269–76
- Petrossians A, Whalen J J, Weiland J D and Mansfeld F 2011b Surface modification of neural stimulating/recording electrodes with high surface area platinum–iridium alloy coatings *2011 Annual Int. Conf. of the IEEE Eng. Med. Biol. Soc.* pp 3001–4
- Randles J E B 1947 Kinetics of rapid electrode reactions *Discuss. Faraday Soc.* **1** 11–9
- Richardson R T et al 2009 Polypyrrole-coated electrodes for the delivery of charge and neurotrophins to cochlear neurons *Biomaterials* **30** 2614–24
- Seligman P 2009 Prototype to product—developing a commercially viable neural prosthesis *J. Neural Eng.* **6** 05006
- Senn P 2015 Neurostimulation for the management of pain *PhD Thesis* University of Melbourne, Australia
- Shepherd R K, Carter P, Enke Y L, Wise A K and Fallon J B 2019 Chronic intracochlear electrical stimulation at high charge densities results in platinum dissolution but not neural loss or functional changes *in vivo* *J. Neural Eng.* **16** 026009
- Shepherd R K, Murray M T, Houghton M E and Clark G M 1985 Scanning electron microscopy of chronically stimulated platinum intracochlear electrodes *Biomaterials* **6** 237–42
- Shepherd R K, Villalobos J, Burns O and Nayagam D A X 2018 The development of neural stimulators: a review of preclinical safety and efficacy studies *J. Neural Eng.* **15** 041004
- Staples N A, Goding J A, Gilmour A D, Aristovich K Y, Byrnes-Preston P, Holder D S, Morley J W, Lovell N H, Chew D J and Green R A 2017 Conductive hydrogel electrodes for delivery of long-term high frequency pulses *Frontiers Neurosci.* **11** 748
- Stöver T and Lenarz T 2009 Biomaterials in cochlear implants *GMS Curr. Top. Otorhinolaryngol. Head Neck. Surg.* **8** Doc10
- Sun B, Li T, Xia K, Zeng Q and Wu T 2017 Flexible microelectrode array for retinal prosthesis *Conf. Proc. IEEE Eng. Med. Biol. Soc.* pp 1097–100
- Tremiliosi-Filho J and Conway B E 1991 Characterization and significance of the sequence of stages of oxide film formation at platinum generated by strong anodic polarization *Langmuir* **8** 658–67
- Troyk P R, Detlefsen D E, Cogan S F, Ehrlich J, Bak M, McCreery D B, Bullara L and Schmidt E 2004 ‘Safe’ charge-injection waveforms for iridium oxide (AIROF) microelectrodes *Conf. Proc. Eng. Med. Biol. Soc.* **6** 4141–4
- van der Horst C, Silwana B, Iwuoha E and Somerset V 2015 Synthesis and characterization of bismuth-silver nanoparticles for electrochemical sensor applications *Anal. Lett.* **48** 1311–32
- Vara H and Collazos-Castro J E 2019 Enhanced spinal cord microstimulation using conducting polymer-coated carbon microfibers *Acta Biomater.* **90** 71–86
- Venkatraman S, Hendricks J, King Z A, Sereno A J, Richardson-Burns S, Martin D and Carmena J M 2011 *In vitro* and *in vivo* evaluation of PEDOT microelectrodes for neural stimulation and recording *IEEE Trans. Neural Syst. Rehabil. Eng.* **19** 307–16
- Verrills P, Sinclair C and Barnard A 2016 A review of spinal cord stimulation systems for chronic pain *J. Pain Res.* **9** 481–92
- Vomero M et al 2018 Incorporation of silicon carbide and diamond-like carbon as adhesion promoters improves *in vitro* and *in vivo* stability of thin-film glassy carbon electrocorticography arrays *Adv. Biosyst.* **2** 1–12
- Wissel K, Brandes G, Putz N, Angrisani G L, Thieleke J, Lenarz T and Durisin M 2018 Platinum corrosion products from electrode contacts of human cochlear implants induce cell death in cell culture models *PLoS One* **13** e0196649
- Woo-Ram L et al 2017 A convex-shaped, PDMS-parylene hybrid multichannel ECoG-electrode array *Conf. Proc. IEEE Eng. Med. Biol. Soc.* pp 1093–6
- Yamato O and Wernet W 1995 Stability of polypyrrole and poly(3,4-ethylenedioxythiophene) for biosensor application *J. Electroanal. Chem.* **397** 163–70
- Zeng F G 2015 Development and evaluation of the Neurotron 26-electrode cochlear implant system *Hear. Res.* **322** 188–99
- Zeng F G, Rebscher S, Harrison W, Sun X and Feng H 2008 Cochlear implants: system design, integration, and evaluation *IEEE Rev. Biomed. Eng.* **1** 115–42